Fluoranthene Based Derivatives for Detection of Trace Explosive Nitroaromatics

ARTICLE *in* THE JOURNAL OF PHYSICAL CHEMISTRY C · APRIL 2013

Impact Factor: 4.77 · DOI: 10.1021/jp3121148

3 AUTHORS, INCLUDING:

Shiv Kumar
Indian Institute of Science
7 PUBLICATIONS **132** CITATIONS
SEE PROFILE

Venkatramaiah Nutalapati
University of Aveiro
43 PUBLICATIONS **452** CITATIONS
SEE PROFILE

THE JOURNAL OF PHYSICAL CHEMISTRY C

Article

pubs.acs.org/JPCC

Fluoranthene Based Derivatives for Detection of Trace Explosive Nitroaromatics

Shiv Kumar,[†] N. Venkatramaiah,[†] and Satish Patil*

Solid State and Structural Chemistry Unit, Indian Institute of Science, Bangalore 560012

Supporting Information

ABSTRACT: A series of fluoranthene derivatives (**F1**−**F5**) varied with nature and type of substituents were synthesized *via* Diels−Alder reaction followed by *in situ* decarbonylation. The solid state structures have been established through single crystal X-ray diffraction (XRD). The presence of extended conjugation and having two alkyloxy chains on phenyl rings induces flexibility to orient opposite to each other and interacts with another fluoranthene unit with weak $\pi-\pi$ interactions and show unique supramolecular arrangements. The envisaged photophysical and DFT studies demonstrated that HOMO−LUMO levels were effectively tuned by different substituents with an optical band gap from 3.44 to 3.88 eV provoked to examine as sensitive fluorescent chemosensors for the detection of nitroaromatic compounds (NACs). The sensitivity toward the detection of NACs was evaluated through fluorescence quenching in solution (aqueous and non-aqueous) and solid state (vapor and contact mode). Fluorescence studies demonstrated that electron transfer occurs from the electron rich fluoranthene fluorophores to the electron deficient NACs by the dominant static quenching mechanism and the quenching process is reversible. It was found that the detection sensitivity increases with extent of conjugation on fluoranthene unit. The contact mode approach using thin layer silica chromatographic plates exhibits a femtogram (1.15 fg/cm^2) detection limit for trinitrotoluene (TNT) and picric acid (PA), while the solution state fluorescence quenching shows for PA detection at the 2−20 ppb level. The sensing performance of fluoranthene thin films to NACs in aqueous solution reveals that fluorophores are highly selective towards the detection of PA. The smart performances of thin film fluorophores with high photostability have great advantage than those of conjugated polymers with superior sensitive detection of PA in groundwater.

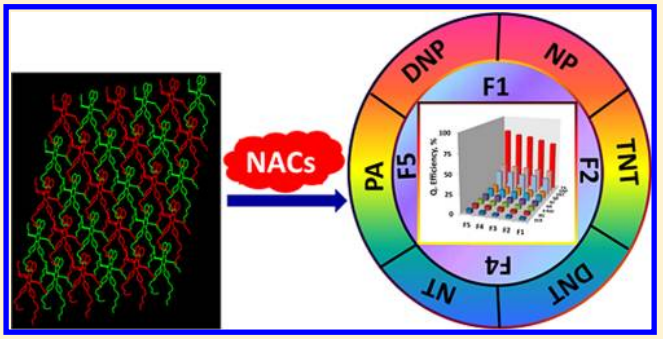

1. INTRODUCTION

In recent years, selective and sensitive detection of explosive nitroaromatic compounds (NACs) has attracted much attention due to national security and also recognized as toxic contaminants for environmental pollution.[1a−d] To enhance the protection of society, investigations of arson, post-blast residue determinations and alleviate for locating buried land mines is an urgent demand.[2a,b] Currently, sniffers (artificial dog's nose) using advanced materials are able to search large areas and to locate explosives by smelling the compounds.[3a−c] It has been found that the picric acid (PA), an organic acid used as an explosive material, and its vapors are hazardous and cause headache, weakness, anemia, and liver injury.[4] Various types of materials were developed and employed to improve the sensing performance of picric acid and other NACs by different analytical tools. Among various analytical methods, fluorescence quenching has been widely employed and proven to be one of the most sensitive and convenient methods over X-ray diffraction, neutron activation, ion mobility spectrometers, and surface enhanced Raman spectroscopy due to its properties of higher sensitivity, selectivity, and operation simplicity.[5a−f] Conjugated polymers become highly attractive for this purpose because of changes in their absorption, emission, and redox properties that can be tuned by variation in the structural modifications.[6a,b] Swager and co-workers first employed the use of various types of conjugated polymers containing three-dimensional pentiptycene moieties in the backbone of poly(*p*-phenyleneethynylene) by intrinsic fluorescence amplification.[7a,b] Later, various types of organic and inorganic conjugated polymers have reported by various research groups. Trogler and co-workers demonstrated that polymetalloles and metallole copolymers are effective materials for building up NAC sensors used both in vapor and solution phases. They also developed a novel cost-effective analytical method by covalent surface attachment of polymers containing silole and silafluorene moieties on thin layer chromatography (TLC) substrates for improved detection of subnanogram traces of explosive residues.[8a−d] Wang et al. have developed conjugated poly(aryleneethynylenesiloles) for the detection of TNT and PA by aggregate-enhanced emission (AEE) effect and aggregation caused quenching (ACQ) effect.[9] Different types of polysiloles exhibit the aggregation induced enhancement effect for

Received: December 9, 2012
Revised: March 6, 2013

   dx.doi.org/10.1021/jp3121148 | *J. Phys. Chem. C* XXXX, XXX, XXX−XXX

detection of NACs in parts per billion (ppb) levels.[10] Recently, Ajayaghosh et al. have reported an attogram level of TNT detection with a perfluoroarene based self-assembled molecular gelator coated on disposable paper strips.[11] Monolayer assembly of polycyclic aromatics with flexible spacers of different chain lengths attached on pyrene units deposited on a glass surface reveals that sensing behavior toward NACs strongly depends on the film thickness, density of the sensing element on the substrate surface.[12a,b] The low permeability of the NACs in the thick films and weak binding strength of the films to the analytes and the energy migration between polymer chains restrict the sensing performance of the films. This renders it difficult to understand the structure−property relationship which is a prerequisite for sensor applications. Hence, development of efficient chemosensors based on small molecule fluorophores has become a more prominent goal of the scientists working in both fundamental and applied research areas due to its well-defined structure, monodispersity, and convenient methods of purification that allow a clear understanding of structure−property relationships. Small molecule based fluorescent sensors for detection of explosives have also been investigated although to a much lesser extent. The strong electron accepting capability of NACs could facilitate a photoinduced electron transfer process with fluorophores. Kim et al. reported bispyrene-appended 1,3-alternate calix[4]arene based small molecule receptors with a TNT detection limit of 1.1 ppb.[13] Anzenbacher and co-workers have developed 1,4-diarylpentiptycenes based simple molecules for the vapor detection TNT by 7.7 ppb level.[14] Wang et al. have developed a colorimetric and fluorescent *N*-acylhydrazone based receptor for specific recognition of picric acid.[15] A series of Zn−Salen complexes were developed and employed for the detection of NACs and showed that quenching occurs through both static and dynamic processes.[16] Different types of π-electron-rich fluorophores functionalized with trimethylsilylethynyl and 3D supramolecular assemblies of metal−organic frameworks were designed for ppb level detection of picric acid.[17a,b] Recently, we have reported a novel fluoranthene based fluorescent chemosensor for picric acid by intercalative interaction between fluoranthene and NACs.[18] The electronic and optical properties can be tuned by extending the conjugation and also by introducing different electron donating substituents on the fluoranthene core. The substituents can facilitate strong electronic communication because of their structural rigidness with a reduced band gap of the material and also favor the formation of strong intermolecular and $\pi-\pi$ interactions with NACs. This results in enhancement of detection sensitivity. In this paper, we report facile synthesis of novel highly fluorescent fluoranthene derivatives with variations in the nature of substituents and carried out a systematic study of their enhanced sensitivity towards the detection of NACs in solution and solid state. The structural modifications on the fluoranthene core and extension of conjugation allowed us to enforce these derivatives with interesting and desirable properties for detection of NACs.

2. EXPERIMENTAL SECTION

2.1. Materials and Measurements. All the nitroaromatics such as picric acid (PA), 2,4,6-trinitrotoluene (TNT), 2,4-dinitrophenol (DNP), 2,4-dinitrotoluene (DNT), 4-nitrophenol (NP), 4-nitrotoluene (NT), nitrobenzene (NB), and 1,3-diphenylacetone (DPA) of analytical grade were obtained from Sigma Aldrich and used directly without further purification.

Caution: TNT and other NACs used in the present study are highly explosive and should be handled only in small quantities.

^{1}H NMR and ^{13}C NMR spectra were recorded on Bruker 400 and 100 MHz NMR spectrometers and calibrated using TMS as an internal reference. Chemical shifts are reported in parts per million (ppm). The UV−vis spectra were recorded on a Perkin-Elmer (Lambda 35) UV−vis spectrometer. All the absorption spectra in solution state were recorded in $CHCl_3$ (conc. 1×10^{-5} mol/L), and the spectra in the solid state were recorded from films of compounds spin coated on quartz substrate. Steady state fluorescence emission studies were carried out with a Spex FluoroLog-3 spectrofluorometer (Jobin-Yvon Inc.). The fluorescence quenching experiments were carried out in a quartz cell in ethanol medium. Stern−Volmer quenching rate constants were estimated by plotting the ratio of I_o/I to the concentration of the quencher [Q], where I_o and I are the maximum fluorescence intensity of the fluorophore before and after addition of analytes, respectively. The thin films were fabricated by taking 2 mg of fluorophore in 0.1 mL of chloroform solution and spin coated on a quartz plate with a rate of 2000 rpm and annealed at 50 °C for 2 h. The fabricated thin film on the quartz plate was kept directly facing the excitation light source, and data collection was made. The position of the film was kept constant during each set of measurements. The solid state fluorescence quenching performance in the vapor phase was tested under saturated vapors of NACs. Time resolved fluorescence measurements were carried out with time-correlated single-photon counting (TCSPC) with nanosecond LED (295 nm) with a repetition rate of 1 MHz used to excite the samples. Single crystal X-ray diffraction data sets were collected on an Oxford Xcalibur (Mova) diffractometer equipped with an EOS CCD detector using Mo Kα radiation (λ = 0.71073 Å). The single crystal was maintained at the desired temperature during data collection using the Oxford instruments Cryojet-HT controller. All structures were solved by direct methods using SHELXS-97 and refined against F2 using SHELXL-97.[19] H-atoms were fixed geometrically and refined isotropically. The WinGX package was used for refinement and production of data tables and ORTEP-3 for structure visualization and making molecular representations showing the ellipsoids at 30% probability level.[20] Analysis of the H-bonding and $\pi-\pi$ interactions was carried out using PLATON, and packing diagrams were generated by using MERCURY.[21] All quantum chemical calculations were carried out in the Gaussian 03 program by using the hybrid function B3LYP with the 6-31g* basis set.[22]

2.2. Synthesis. The synthesis of different substituted diphenylacetylene derivatives such as 1,2-diphenylacetylene (**P1**), 1,2-bis(4-(hexyloxy)phenyl)ethyne (**P2**), 1,3-bis(4-bromophenyl)propan-2-one (**P3**), 7,9-diphenyl-8H-cyclopenta-[a]acenaphthylen-8-one (**P4**), 7,9-bis(4-bromophenyl)-8H-cyclopenta[a] acenaphthylen-8-one (**P5**), and fluoranthene derivatives (**F1**−**F3**) were described in the Supporting Information.

*2.2.1. Synthesis of 7,10-Bis(4-butylphenyl)-8,9-bis(4-(hexyloxy)phenyl)fluoranthene (**F4**).* The compound **F3** (0.4 g, 0.46 mmol) was taken in a 100 mL round-bottom flask, and *n*-butyllithium (1.6 M in hexane, 1.0 mmol) was added dropwise over a period of 15 min in dry THF under an argon atmosphere at −78 °C. The reaction mixture was allowed to attain room temperature and stirred at this temperature for

dx.doi.org/10.1021/jp3121148 | J. Phys. Chem. C XXXX, XXX, XXX−XXX

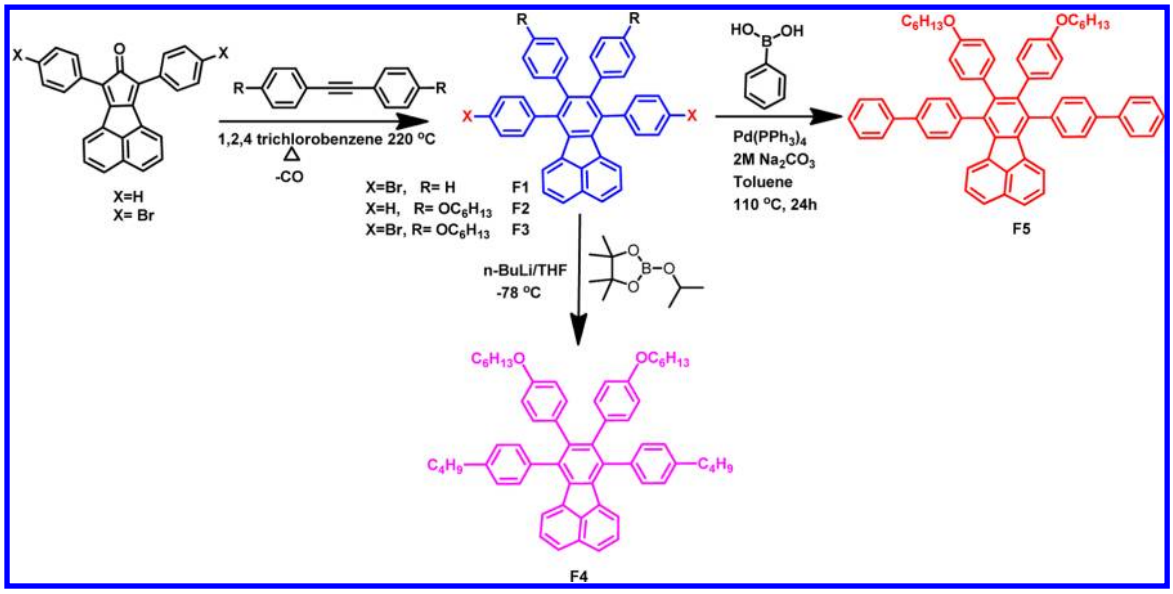

Figure 1. Schematic representation of synthesis of fluoranthene derivatives (**F1**−**F5**).

45 min. 2-Isopropoxy-4,4,5,5-tetramethyl-1,3,2-dioxaborolane (0.43 g, 2.3 mmol) was added under vigorous stirring at −78 °C. After addition, the reaction mixture was brought to room temperature and stirred overnight. Solvent was evaporated under reduced pressure. The residue was extracted with a dichloromethane/water mixture. The organic layer was dried over anhydrous sodium sulfate, subjected to evaporation; the residue was loaded into a silica gel column with 5% ethylacetate/hexane as eluent (20% yield). ^{1}H NMR (400 MHz, $CDCl_3$, TMS, ppm): 7.67 (d, J = 8.1 Hz, 7H), 7.30−7.22 (m, 10H), 7.18 (d, J = 8.1 Hz, 14H), 7.11 (d, J = 8.1 Hz, 14H), 6.79−6.73 (m, 14H), 6.60 (d, J = 7.0 Hz, 7H), 6.45−6.40 (m, 14H), 3.75 (t, J = 6.7 Hz, 15H), 2.64 (t, J = 7.5 Hz, 15H), 1.70−1.59 (m, 31H), 1.42−1.23 (m, 75H), 0.95 (t, J = 7.3 Hz, 21H), 0.88 (t, J = 6.9 Hz, 20H). ^{13}C NMR (100 MHz, $CDCl_3$, TMS, ppm): 156.53, 141.08, 140.70, 137.56, 137.37, 136.84, 136.44, 133.29, 132.52, 132.32, 129.88, 129.58, 128.21, 127.52, 126.19, 123.04, 112.81, 77.32, 77.00, 76.68, 67.71, 35.34, 33.48, 31.62, 29.69, 29.23, 25.68, 22.56, 22.11, 14.01. Elemental Analysis ($C_{60}H_{66}O_2$): Calcd (%): C, 87.97; H, 8.12; O, 3.91.

*2.2.2. Synthesis of 7,10-Di([1,1′-biphenyl]-4-yl)-8,9-bis(4-(hexyloxy)phenyl)fluoranthene (**F5**).* Compound **F3** (0.2 g, 0.23 mmol) and phenyl boronic acid (60 mg, 0.46 mmol) were dissolved in a mixture of toluene (30 mL) and 2 M sodium carbonate aqueous solution (2 mL). The mixture was stirred at 90 °C under an argon atmosphere followed by the addition of $Pd(PPh_3)_4$ (10 mg). After vigorous stirring for 24 h, the resulting mixture was extracted with dichloromethane (30 mL). The organic layer was dried over anhydrous sodium sulfate and subjected to solvent evaporation. The obtained solid residue was loaded into a silica gel column with 5% ethylacetate/hexane as eluent to give **F5** (50% yield). ^{1}H NMR (400 MHz, $CDCl_3$, TMS, ppm): 7.70 (d, J = 8.2 Hz, 6H), 7.61 (d, J = 8.0 Hz, 4H), 7.47 (t, J = 7.6 Hz, 4H), 7.40−7.32 (m, 6H), 7.28 (t, J = 7.6 Hz, 2H), 6.81 (d, J = 8.5 Hz, 4H), 6.73 (d, J = 7.1 Hz, 2H), 6.45 (d, J = 8.5 Hz, 4H), 3.74 (t, J = 6.7 Hz, 4H), 1.68−1.59 (m, 4H), 1.35 (dd, J = 14.7, 6.6 Hz, 6H), 0.87 (dd, J = 13.3, 6.6 Hz, 12H). ^{13}C NMR (100 MHz, $CDCl_3$, TMS, ppm): 156.66, 140.75, 140.74, 139.27, 139.08, 137.34, 136.60, 136.44, 132.28, 132.22, 130.38, 128.79, 127.63, 127.25, 126.91, 126.69, 126.43, 122.14, 112.93, 77.32, 77.00, 76.68, 67.68, 31.92, 31.61, 29.69, 29.20, 25.65, 22.68, 22.54, 14.00, 13.98. Elemental analysis ($C_{64}H_{58}O_2$): Calcd (%): C, 89.47; H, 6.80; O, 3.72. Found (%): C, 87.15; H, 7.33.

3. RESULTS AND DISCUSSION

As illustrated in Figure 1, the synthetic route describes the synthesis of various fluoranthene derivatives (**F1**−**F5**) by varying the substituents −Br, alkoxy chain ($-OC_6H_{13}$) on the phenyl rings of fluoranthene and extended conjugation by replacing −Br with phenyl ring. The use of long alkoxy chains enhances the solubility of fluoranthene derivatives and hinders the formation of aggregation and excimer. Acetylene derivatives **P1** and **P2** were synthesized by the Sonogashira cross coupling reaction. Cyclopentadienone derivatives **P4** and **P5** were obtained in good yields according to the known literature.[24] Compound **F1** was synthesized by Diels−Alder reaction between 7,9-bis(4-bromophenyl)-8*H*-cyclopenta[a]-acenaphthylen-8-one, **P5**, and 1,2 diphenylacetylene in 1,2,4-trichlorobenzene in a sealed glass pressure tube, affording **F1** in 60% yield. A similar methodology was employed for the synthesis of **F2** and **F3** by taking the corresponding cyclopentadienone and diphenylacetylene derivatives. To have a better understanding and to compare the fluoranthene based small molecules to the polymers toward the implications in chemosensors for NACs, attempts were made to develop the polymer of **F3**. Prior to the polymerization of **F3**, we attempted to convert dibromo derivative of **F3** into boronic ester/acid for Suzuki coupling reaction. The use of *n*-butyllithium at −78 °C is the ideal reaction conditions reported in the literature for the synthesis of the various boronic acids and esters. We employed similar conditions as described in Figure 1 for the formation of boronic ester of **F3**. However, it is surprising to see the formation of **F4** by replacing bromine atom with the butyl chain.[25] The structure of **F4** was confirmed by NMR and single crystal X-ray analysis. Thus, we extended the conjugation by Suzuki cross coupling reaction between **F3** and phenyl boronic acid in the presence of $Pd(PPh_3)_4$ in a catalytic amount yields the formation of compound **F5** in 50% yield. All the new diverse fluoranthene derivatives show good solubility in many of the organic solvents. The detailed characterization of these

dx.doi.org/10.1021/jp3121148 | J. Phys. Chem. C XXXX, XXX, XXX−XXX

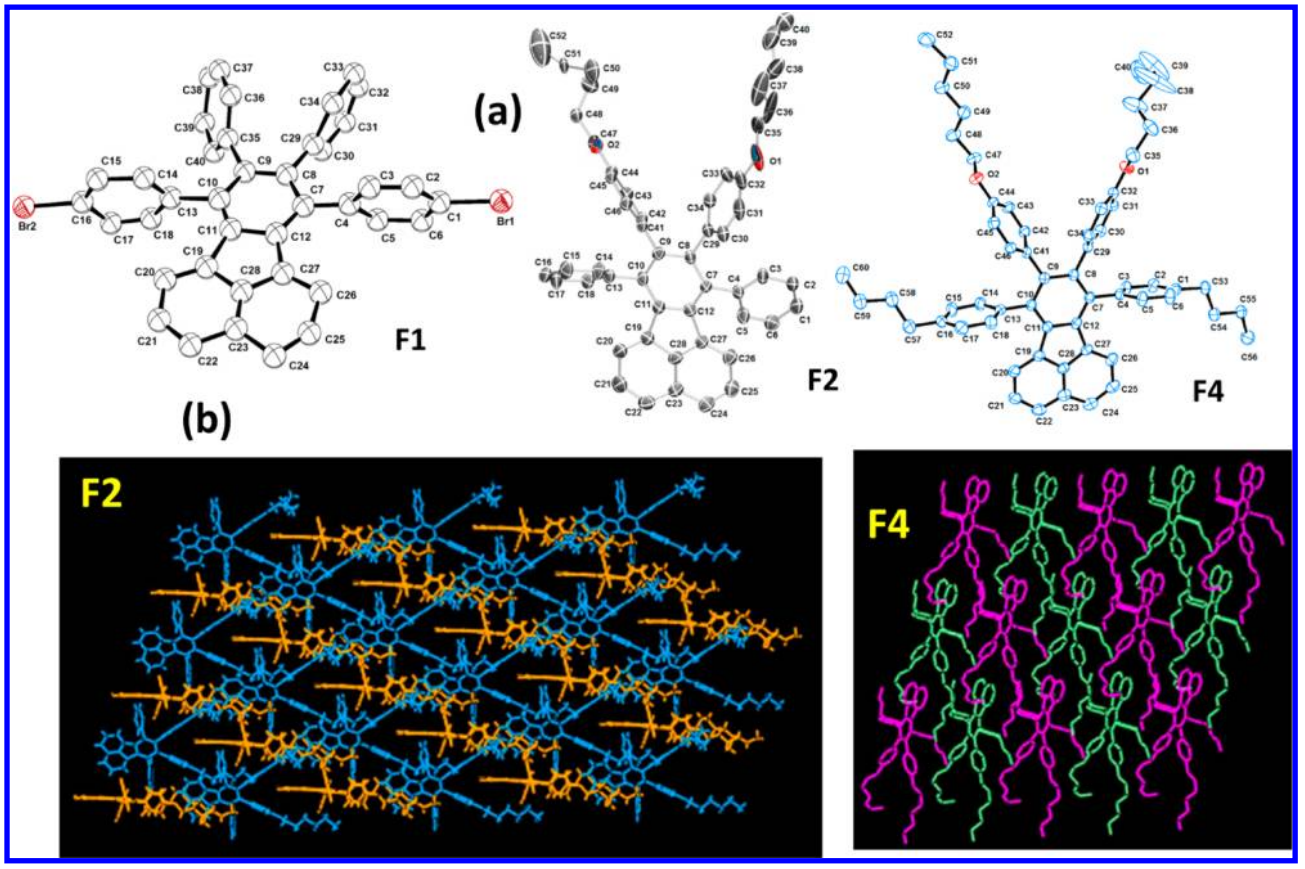

Figure 2. (a) ORTEP diagrams **F1**, **F2**, and **F4** drawn at 30% probability ellipsoids. (b) Supra-molecular arrangement of **F2** and **F4**.

derivatives by ^{1}H and ^{13}C NMR, and single crystal X-ray analysis is provided in the Supporting Information.

3.1. Single Crystal X-ray Analysis. For single crystal X-ray analysis, high quality crystals were obtained by the slow solvent evaporation method in dichloromethane/ethanol mixtures at ambient temperature. The compound **F2** exhibits triclinic space group $P\bar{1}$ with $Z = 2$, while the compounds **F3** and **F4** exhibit monoclinic space group $P2_1/c$ with $Z = 4$ and structures are determined from the crystal data collected at 110 K by single crystal XRD. The compound **F1** forms light yellow crystals with opaque nature, and the quality of the crystals was poor. The unit cell shows the presence of eight molecules with disorder in the unit cell which makes it difficult for the refinement. Thus, we have provided an *ORTEP* diagram of **F1** without having complete refinement and fully refined structures of **F2** and **F4** are shown in Figure 1.

Since, all the fluoranthene derivatives (**F1**−**F5**) having a common fluoranthene unit and the variations in the structural arrangements in the solid state are purely governed by substituents on phenyl rings. In the solid state, the compound **F2** is strongly stabilized by C−H···π (2.88 Å) interactions involving alkylated C−H and the phenyl ring of adjacent **F2** units and has O···H (2.685 Å) interactions. The supramolecular arrangement along the *ab* plane is shown in Figure 2b. The presence of two alkyl chains on the phenyl ring becomes so flexible to orient opposite to each other and creates a cavity to enter another fluoranthene unit with very weak π−π interaction (7.412 Å). The crystal structure of compound **F3** exhibits similar to **F2** in all respects expect the molecular assembly and intermolecular interactions.[23] The compound **F4** forms greenish yellow crystals with monoclinic $P2_1/c$ space group. We have observed two nonequivalent types of C−H···π (2.609 Å) involving alkylated C−H and the phenyl ring of adjacent **F4** units and another C−H···π (2.81 Å) between two phenyl rings. The presence of butyl chains on phenyl rings at C_1 and C_{16} positions makes the fluoranthene core in more planar nature with weak π−π interactions (7.641 Å). The supramolecular assembly shows interesting structural features of well-organized humanoid-like motifs along the *ab* plane. In the solid state, all molecules exhibit either bent or twisted conformations of the fluoranthene backbone. The degree of bending can be determined by analyzing the dihedral angle and the bent angle between the two peripheral benzene and central fluoranthene unit. For **F2**, the torsional angles of C_7−C_8−C_{29}−C_{34} show 111.55° while the other phenyl ring C_{10}−C_9−C_{41}−C_{42} shows a torsional angle of 107.25°. The bent angle at C_7−C_8−C_{29} is found to be 117.55°, and the bent angle at the C_{10}−C_9−C_{41} position is 120.28°. This clearly shows that the mean plane of the fluoranthene unit is twisted by the presence of phenyl rings. However, this pronounced effect is less in comparison to **F3** as described earlier.[23] For compound **F4**, the torsional angles are found to be 109.59° for C_7−C_8−C_{29}−C_{34} and 94.21 for C_{10}−C_9−C_{41}−C_{42}. The presence of flexible butyl chains on phenyl rings at the C_1 and C_{16} positions reduces the bent angle and makes them more coplanar with the fluoranthene core. The change in torsional angles indicates that the relative conformation of the backbone is affected by the choice of substituent.

3.2. Photophysical Properties. The optical absorption spectra of fluoranthene derivatives in chloroform and thin films are shown in Figure 3. In solution (Figure 3a), all of the compounds exhibit two well resolved major intense absorption

dx.doi.org/10.1021/jp3121148 | J. Phys. Chem. C XXXX, XXX, XXX−XXX

Table 1. Summary of Photophysical Data for Various Fluoranthene Derivatives in Chloroform and Thin Films

	optical absorption (nm)		fluorescence emission (nm)			Stoke's shift (nm)		optical band gap (eV)			
S.No	sol	thin film	sol	Q.Y.	thin film	sol	thin film	sol	thin film	HOMO−LUMO gap (eV)	lifetime (ns)
F1	301, 333, 374	305, 333, 387	476	26.1	475	102	88	3.03	2.56	3.88	8.23
F2	301, 333, 375	300, 335, 376	477	31.4	476	102	100	3.05	3.02	3.77	11.23
F3	301, 332, 375	300, 334, 376	477	31.6	476	101	100	3.05	3.01	3.62	11.37
F4	300, 333, 375	300, 335, 377	478	33.4	481	103	95	3.09	2.92	3.54	11.87
F5	297, 332, 371	289, 333, 376	471	27.1	466	100	90	3.10	2.88	3.44	11.68

bands at ∼297 ± 2 and ∼374 ± 2 nm, which arise due to $\pi \rightarrow \pi^*$ transitions. The maximum absorption peak for compound **F5** is slightly blue-shifted by 4 nm in comparison to **F1** and **F2** and becomes more broaden. It suggests that outer phenyl rings do not extend the conjugation of the core dramatically. In thin films, the absorption pattern of compound **F1** is more broadened with a decrease in the intensity and red-shifted by ∼13 nm, while compound **F5** is blue-shifted (major $\pi \rightarrow \pi^*$ transition) by ∼8 nm in comparison with the solution. In principle, increasing conjugation of the aromatic π-system should cause the bathochromic shift in absorption bands. Since the rotation of the benzene ring is perpendicular to the mean plane of the fluoranthene unit, it causes the loss of the electron exchange contribution as observed similar to the biphenyl system.[26] The appearance of a red shift and broad absorption in solid state for **F1** arises due to its symmetrical nature and having strong intermolecular interactions. The absorption profiles of all fluoranthene derivatives are quite similar in both cases with well resolved vibronic bands in the lower energy side of the spectra. From the low energy onset of the absorption bands, the optical band gaps were calculated and presented in Table 1. It is evident from the data listed in Table 1 that the energy gap of these materials can be fine-tuned by appropriate substitution. The optical band gaps were found to be in the range 3.03−3.1 eV in solution and show small variations in solid state that depend on the nature of substituents. In the solid state, the optical band gaps for **F1**, **F2**, **F4**, and **F5** are found to be 2.56, 3.02, 2.92, and 2.88 eV, respectively. All fluoranthene derivatives exhibit strong blue emission (Figure 3b) at ∼475 nm with a Stokes' shift of 103 ± 2 nm. The emission spectrum of **F5** is slightly blue-shifted in comparison to other fluoranthene derivatives. The relative emission intensity of **F2** is found to be lesser due to the presence of bromine groups as heavy atom effect. The variations in the spectral pattern arise due to the change in the conformational relaxation occurring in the excited state process before emission takes place. The fluorescence quantum yield (Φ) of all the derivatives exhibits in the range 26−34% in chloroform. The pertinent data of quantum yields are summarized in Table 1.

The fluorescence lifetime (Figure 3c) of **F1**−**F5** in chloroform is found to be in the range 8.23−11.87 ns by the time correlated single photon counting (TCSPC) method. The pertinent results of photophysical and fluorescence lifetime data on the effect of the substituents with the extension of the aromatic system were analyzed and summarized in Table 1. On the basis of the spectral evidence, we infer that the structures of fluoranthene derivatives are quite similar in solution as well in solid state.

NACs are known to be high electron deficient molecules and undergo strong interactions with nearby excited fluorescent species. The high stability and electron rich environment of fluoranthene derivatives make an ideal candidate to probe the sensing of explosive NACs by the fluorescence quenching technique. All fluoranthene derivatives (**F1**−**F5**) were treated with different NACs such as picric acid (PA), 2,4,6-trinitrotoulene (TNT), 2,4-dinitrotoulene (DNT), 2,4-dinitrophenol (DNP), and common interfering electron deficient molecules like 1,4-dichlorobenzene (DCB), benzoquinone (BQ), and other analytes. Solution state fluorescence quenching experiments were carried out by titration of fluoranthene derivative solutions (1.0×10^{-6} M) with known concentrations of explosive NACs. Due to the electron transfer process between the fluoranthene and the explosive NACs molecules, the fluorescence intensity is readily quenched upon gradual addition.

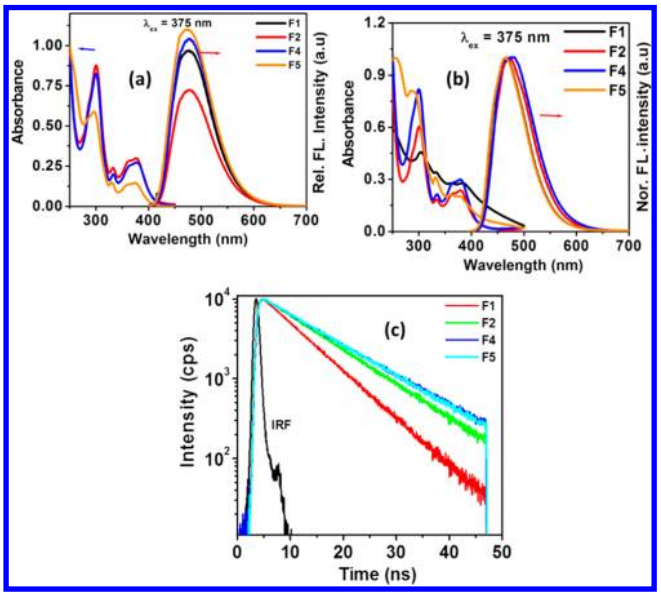

Figure 3. The optical absorption and emission spectra of different fluoranthene derivatives: (a) solution, (b) thin films, (c) fluorescence lifetime decay profiles of fluoranthene derivatives in chloroform.

Figure 4 shows the fluorescence quenching behavior of **F5**, upon gradual addition of 10 μL of 0.1 mM solution PA. The quenching behaviors of other fluoranthene derivatives with different NACs are provided in the Supporting Information (Figure S2). Upon gradual addition of different concentrations of PA to **F5**, the fluorescence intensity at ∼469 nm is dramatically decreased and shows 90% quenching for 10 μM PA. The quenching behavior was analyzed by the Stern−Volmer (SV) formalism $I_o/I = 1 + K_{SV}[Q]$, where I_o and I are the fluorescence intensities in the absence and presence of the quencher [Q] and K_{SV} is the Stern−Volmer rate constant. The decrease in the fluorescence intensity could be an electron

dx.doi.org/10.1021/jp3121148 | J. Phys. Chem. C XXXX, XXX, XXX−XXX

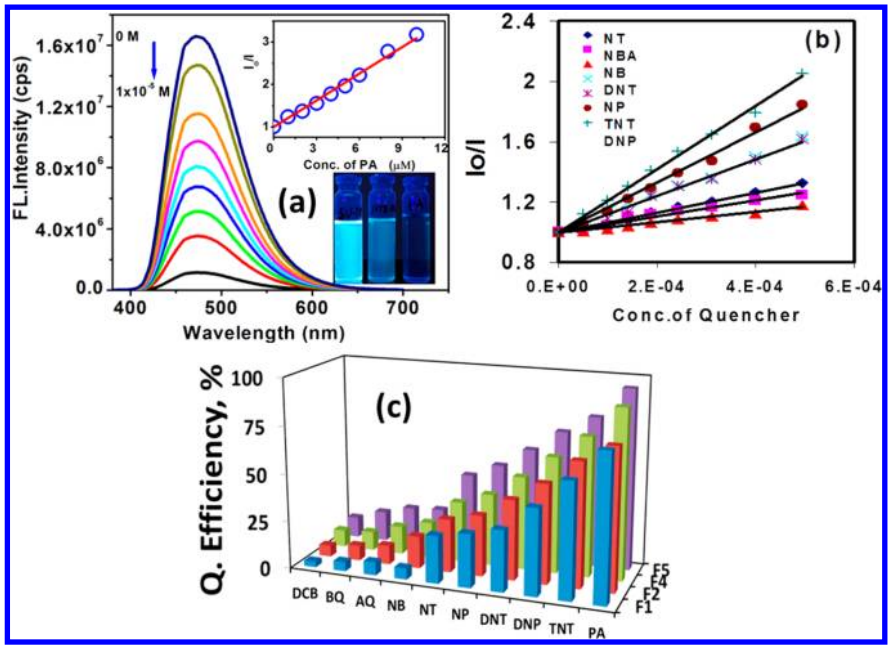

Figure 4. (a) Fluorescence quenching behavior of **F5** with gradual addition of PA in ethanol. The inset shows the Stern–Volmer plot of **F5** with different concentrations of PA. The inset photograph shows the change in the fluorescence intensity at **F5** before and after addition of PA. (b) Stern–Volmer plot of various fluoranthene derivatives treated with various analytes at different concentrations. (c) Quenching efficiency of various fluoranthene derivatives for different analytes.

transfer process on the basis of thermodynamic considerations as static and dynamic quenching. The inset in Figure 4a shows a linear SV plot for **F5** treated with different concentrations of PA. This indicates the formation of static quenching through a one-to-one nonfluorescent ground state complex, which after excitation returns to the ground state without emission of light. Figure 4b shows the linear behavior of SV plot for **F5** with other NAC analytes. Similar results were observed for other fluoranthene derivatives treated with different nitroaromatic analytes (Figure S3, Supporting Information). PA exhibits the highest quenching response at parts per billion levels (2–20 ppb), while DNT and TNT show ~1.1 ppm level of detection in solution. The quenching rate constants were found to be high for picric acid $2.405 \times 10^5\ M^{-1}$ for **F5** and follow the order **F5** > **F4** > **F3** > **F2** > **F1**. However, when **F5** is treated with high electron deficient molecules like 9,10-phenanthrenequinone (PAQ) and 1,2-acenaphthylenedione (ANQ), the SV plot shows linear behavior at low concentrations and nonlinear upward curvature at high quencher concentrations (Figure S4, Supporting Information). This indicates the presence of both static and dynamic quenching behavior. The formation of dynamic quenching is governed by excited state collisions between **F5** and quenchers. Figure 4c shows the quenching efficiency of **F1**–**F5** with common analytes such as 1,4-dichlorobenzene (DCB), toluene, and benzoquinone (BQ). To our interest, we have not observed any significant decrease in the fluorescence intensity, suggesting that these fluoranthene derivatives are sensitive and selective for the detection of NACs. The formation of a ground state complex between fluoranthene derivatives and NACs is further confirmed by time-resolved fluorescence, spectrophotometric, and NMR titration experiments. The fluorescence lifetime of **F5** at different concentration ratios of PA (Figure S5, Supporting Information) is found to be invariant, which suggests the formation of a ground state complex between **F5** and PA. The ^{1}H NMR spectra of **F1** in $CDCl_3$ with different concentrations of PA are shown in Figure S6a, Supporting Information. Upon gradual addition of PA to **F1** (0.25:1 mol ratio), the doublet peak at 6.68 ppm shows an upfield shift and the intensity of the triplet peak at 7.35 ppm is reduced. With further increases in the mole ratio to 0.5:1 and above, we have observed a gradual upfield shift of the doublet from 7.75 to 7.73 ppm, while the other doublet shows the downfield shift from 6.68 to 6.65 ppm. This clearly shows the presence of strong π–π intermolecular interactions between **F1** and PA. The ^{1}H NMR spectra of **F5** treated with different concentrations of PA are provided in Figure S6b, Supporting Information. Similar behavior in the NMR spectra was observed for other fluoranthene derivatives treated with PA.

The spectrophometric titration of various fluoranthene derivatives with different concentrations of picric acid (PA) in ethanol is shown in Figure S7, Supporting Information. For example, with the gradual addition of PA to **F5**, we have observed a slight increase in the absorption maxima at 303 nm with formation of a new broad absorption peak at 465 nm. The intensity of the new absorption peak gradually increases with an increase in the concentration of PA. Since all of the compounds exhibit similar absorption patterns and show similar spectral variations, this indicates the formation of donor–acceptor complexes between the π-electron rich fluoranthene derivatives and picric acid. As described earlier, for electron transfer based fluorescence quenching, the lowest unoccupied molecular orbital (LUMO) levels of the quenchers and the highest occupied molecular orbital (HOMO) levels of the fluorophores play a crucial role and thereby the frontier molecular orbitals of fluoranthene derivatives were calculated and the results are presented in Figure 5.

Geometry optimization of all derivatives was carried out with the Gaussian 03 program with the B3LYP/6-31g* basis sets. For the compounds **F2**–**F5**, the HOMO orbitals are largely delocalized on the alkoxy substituted phenyl rings attached to fluoranthene and LUMO orbitals are delocalized on the

dx.doi.org/10.1021/jp3121148 | J. Phys. Chem. C XXXX, XXX, XXX–XXX

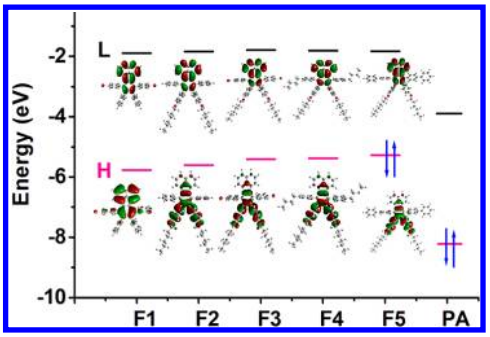

Figure 5. Electron density distribution profiles of LUMO and HOMO of various fluoranthene derivatives optimized with the B3LYP/6-31g* basis set.

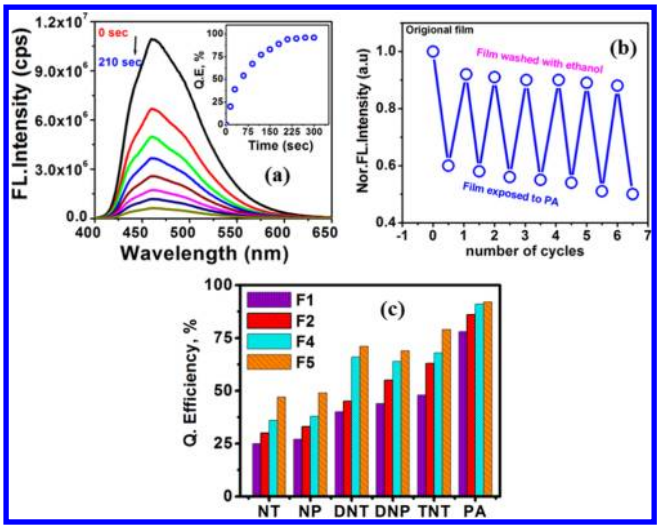

Figure 6. Fluorescence quenching behavior of **F5** thin film upon exposure to saturated vapors of PA at different time intervals. The inset shows the variations in the quenching efficiency of **F5** with respect to different times (b). The reversibility of **F5** thin film to the saturated vapors of PA for 60 s of exposure time. (c) The fluorescence quenching efficiency of fluoranthene derivatives upon exposure to saturated vapors of various NACs.

fluoranthene backbone. For **F1**, HOMO and LUMO orbitals are π-type and mainly localized on the fluoranthene core, which suggests that energy transitions originated from $\pi \rightarrow \pi^*$ transitions. Fluorescence quenching involves the electron transfer process from the LUMO of the excited state fluorophore to the LUMO of the NACs. Detection limits are based on the efficiency of this process, which can be improved by increasing analyte−fluorophore binding interactions and matching the frontier molecular orbital energies of the fluorophore with the LUMO of the NACs. In our previous work,[23] we have shown analyte−fluorophore binding interactions in which analyte molecules enter into the cavity created by substituted phenyl rings of fluoranthene and stabilized by strong intermolecular and $\pi-\pi$ interactions. From the energy level diagram, we could observe that the optical band gaps are in the range 3.88−3.45 eV and show slight variation depending upon the type of substituents present on the fluoranthene unit. On comparison of the optical band gap values determined experimentally and theoretically, they were found in good agreement to support the theoretical molecular geometries. The optical band gap of **F5** is found to be less compared to other derivatives due to an increase in conjugation. The LUMO energy of **F5** is close to the NACs, which could be the major driving force for the electron transfer process with high sensitivity compared to other fluoranthene derivatives. In order to demonstrate the practical use of fluoranthene derivatives for NAC detection, quenching studies were carried out in the solid state by making thin films of fluoranthene derivatives. The thin films of all fluoranthene derivatives were fabricated by the spin coating technique on a quartz substrate with a rate of 2000 rpm and concentration of 1 mg/0.2 mL in chloroform solution. The obtained films were annealed at 50 °C for 2 h. The fluorescence response of the thin films to the vapors of NACs was ascertained by inserting the film into the sealed vials containing solid analytes at room temperature. The detection limits of saturated vapors of NACs were determined according to the standard methodology, as described by Swager et al.[1a,3a] The solid state fluorescence quenching of fluorophore with explosive vapors is known to depend on a series of factors such as the thermodynamic driving force for the electron transfer, strength of electrostatic interactions developed between the fluorophore and the quencher, and the vapor pressure of the analyte. Figure 6a shows the time dependent fluorescence quenching of **F5** thin film exposed to saturated vapors of PA (ca. 2 ppb). The fluorescence intensity was gradually decreased as a function of exposure time and shows 40% decrease in fluorescence intensity for 60 s of exposure time. For 210 s exposure of the saturated vapors of PA, the fluorescence intensity was found to be decreased by 91%. The inset in Figure 6a shows the decrease in the fluorescence intensity with respect to time. This indicates that, with further increase in the exposure time above 210 s, quenching becomes saturated and reaches equilibrium.

Figure 6b shows the reversibility of the **F5** film toward the exposure of PA. The film was exposed to saturated vapors of PA at room temperature for 60 s, and the emission spectrum was recorded. The film was washed with ethanol and dried at 45 °C under a vacuum, and the emission spectrum was recorded again and the whole process was repeated. The results show that the initial fluorescence intensity was significantly retained after several washings, indicating high photostability of the film. The quenching efficiency of 85% was observed even after six cycles of exposure to PA vapors. Similar results were observed for other fluoranthene derivatives and the quenching behavior provided in Figure S8, Supporting Information. All the fluoranthene derivatives show fluorescence quenching behavior to the vapors of other NACs such as DNT, DNP, NP, and NT. However, the extent of quenching is smaller when compared to picric acid and is shown in Figure 6c. The high sensitivity toward the detection of PA follows the order **F5** > **F4** > **F3** > **F2** > **F1**.

NACs are known to be environmental contaminants that pollute soil and drinking water. The recycling ability studies revealed that all the fluoranthene thin films are found to be highly photostable at room temperature and exposed to the saturated vapors of NAC analytes. From this point view, the sensing performance of fluoranthene films in potable water containing low concentrations of nitroaromatics is of great relevance. The thin films were immersed into pure water for 2 h to test the leaking of the fluorophore from the quartz surface which was monitored by measuring the fluorescence emission. Considering the fact that the fluorophore is highly fluorescent, no significant emission from the remaining solvent may indicate that leaking of fluoranthene from the quartz surface is

dx.doi.org/10.1021/jp3121148 | J. Phys. Chem. C XXXX, XXX, XXX−XXX

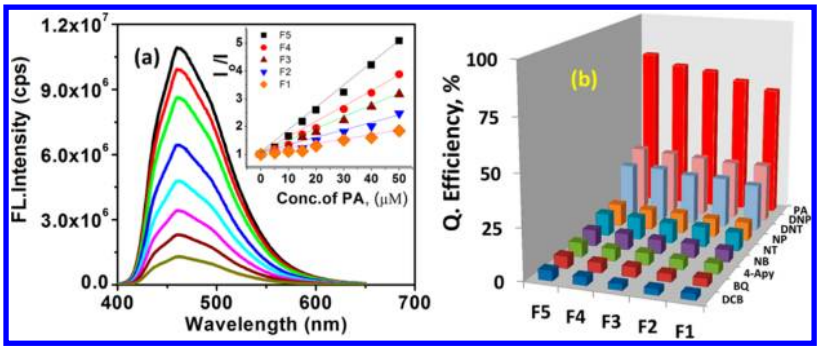

Figure 7. Fluorescence sensing performance of fluoranthene thin films in aqueous solution. (a) Fluorescence emission spectra of the **F5** thin film in the aqueous solution containing different concentrations of PA (0−50 μM). The inset shows the Stern−Volmer plots of various fluoranthene derivatives treated with different concentrations of PA. (b) Quenching efficiencies of various fluoranthene derivative (F1−F5) thin films with different NACs and with common interferents.

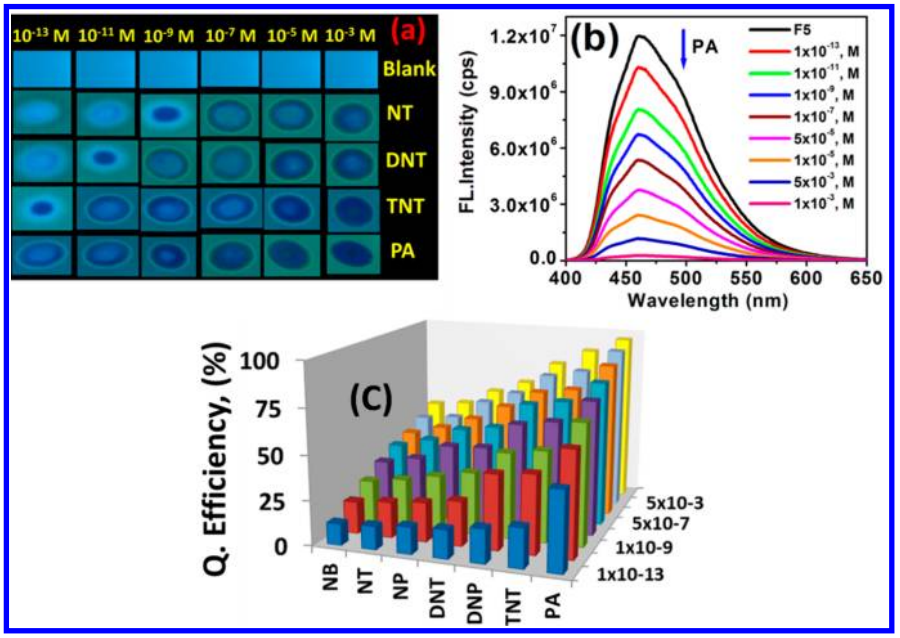

Figure 8. (a) The photograph of **F5** coated on the thin layer silica chromatographic plates before and after addition of different concentrations of various NACs by contact mode with a spot area of ~0.2 cm^2 upon exposure to the UV lamp at 365 nm. (b) Change in the fluorescence intensity of the **F5** coated TLC plate (λ_{ex} = 375 nm) against different concentrations of PA (1×10^{-13}−1×10^{-3} M). (c) Quenching efficiency of various NACs to the fluorescence emission of **F5** coated TLC plates.

negligible. Figure 7a depicts the fluorescence emission spectra of **F5** thin film at various PA concentrations in an aqueous medium. It can be seen that the fluorescence emission intensity was quenched by 79% when the concentration of PA reached 50 μmol/L. The quenching behavior is further studied by the Stern−Volmer equation as described earlier and shows static quenching behavior with a rate constant (K_{sv}) of 7.96×10^4 M^{-1}. The inset in Figure 7a shows the comparison of rate constants of all fluoranthene derivatives, and the rate constants are found to be 1.58×10^4, 2.67×10^4, 4.22×10^4, and 5.49×10^4 M^{-1} for **F1**, **F2**, **F3**, and **F4**, respectively. The selectivity of the films in aqueous medium was further extended to other NACs and other common interfering analytes. Figure 7b shows the histograms of (I_o/I) to the concentrations of PA and its common interferents. It was found that the common interferents like DCB, BQ, and other NACs like NB, NT, NP, and DNT have very little effect on the fluorescence intensity and PA shows the greatest quenching, indicating it is highly selective.

Recently contact mode approach for the testing range of explosive NACs have received great attention for real time applications to find residual contaminations.[8c,11,16] Therefore, we have made an attempt to study the surface sensing approach to test the viability by coating fluoranthene derivatives on thin layer silica chromatographic plates (200 μm). The thin layer silica chromatographic plates exhibit a highly porous nature, and the analyte molecules can easily diffuse into silica plates.

The visual change in the fluorescence intensity will provide the relevance for the onsite instant detection of explosives. For this purpose, 2 mg of fluoranthene derivatives were dissolved in 0.2 mL of chloroform solution and spread over the silica plate by the drop casting method. A 5 μL portion of different concentrations of various NACs (10^{-15}−10^{-3} M concentration range) was spotted on a fluoranthene derivative coated silica plate to give a spot area of ~0.2 cm^2. The visual fluorescence response for different analytes at different concentration levels upon exposure to UV light at 265 nm is shown in Figure 8a. The fluorescence spectra at each film at different concentrations were measured on excitation at λ_{ex} = 375 nm. The formation of

dx.doi.org/10.1021/jp3121148 | J. Phys. Chem. C XXXX, XXX, XXX−XXX

black spots and decrease in the fluorescence intensity as a function of concentration and the minimum detection limit of TNT and PA detectable by the naked eye are as low as 5 μL of 1×10^{-13} M solution with a detection limit of ~1.15 fg/cm^2. Figure 8b shows the fluorescence quenching behavior of **F5** coated TLC plates for different concentrations of PA solution. We have observed 18 and 29% of quenching for 1×10^{-13} M solutions of TNT and PA, respectively. The experiments were repeated for all fluoranthene derivatives for different NACs. A comparison of the fluorescence quenching efficiency for different NACs analytes is shown in Figure 8c. The quenching effect is found to be higher for TNT and PA compared with the other NACs. Similar results were observed for other fluoranthene derivatives, and **F5** shows the highest decrease in the fluorescence intensity with intense black color.

4. CONCLUSION

In conclusion, we have successfully synthesized a series of novel fluoranthene fluorophores varied with nature and type of substituents. The single crystal XRD study reveals a unique supramolecular arrangement of fluoranthene molecules demonstrates promising materials for the sensitive fluorescent chemosensors toward the detection of NACs. The photophysical and computational study demonstrate that tuning of the optical gap with an increase in conjugation enhances the sensitivity of NACs. Solution phase fluorescence study reveals that these fluorophores exhibit static quenching with a 2−20 ppb level of detection for picric acid, while TNT exhibits ~1.1 ppm level. Vapor phase sensing of NACs show fast detection of picric acid in 60 s in the order **F5** > **F4** > **F3** > **F2** > **F1**. Femtogram detection levels for PA and TNT (~1.15 fg/cm^2) were achieved by the contact mode approach on thin layer silica chromatographic plates. For aqueous phase sensing, the fast and efficient response of the film to PA has been attributed to the high diffusion of picric acid into the porous nature of fluoranthene films and forms strong intermolecular interactions. The high blue light emitting nature of fluoranthene derivatives in solution and solid state with high photostability probe to develop switchable turn off/on optoelectronic device is underway.

■ ASSOCIATED CONTENT

Supporting Information

Detailed description of synthetic procedures and their spectral characterization, NMR and UV−visible titrations and fluorescence quenching experiments with various analytes, and single crystal X-ray information along with CCDC 903375 and CCDC 903376. This material is available free of charge via the Internet at http://pubs.acs.org.

■ AUTHOR INFORMATION

Corresponding Author

*Phone: +91-80- 22932651. Fax: +91-80-23601310. E-mail: satish@sscu.iisc.ernet.in.

Author Contributions

†S.K., N.V.: These authors made equal contributions to this work.

Notes

The authors declare no competing financial interest.

■ ACKNOWLEDGMENTS

The authors gratefully acknowledge NMR Research Centre, IISc, for NMR spectra. We also thank Mr. K. Durga Prasad and Prof. T. N. Guru Row, SSCU, IISc, Bangalore, for single crystal XRD analysis.

■ REFERENCES

(1) (a) Yang, J.-S.; Swager, T. M. Fluorescent Porous Polymer Films as TNT Chemosensors: Electronic and Structural Effects. *J. Am. Chem. Soc.* **1998**, *120*, 11864−11873. (b) Salinas, Y.; Martinez-Manez, R.; Marcos, M. D.; Sancenon, F.; Costero, A. M.; Parra, M.; Gil, S. Optical Chemosensors and Reagents to Detect Explosives. *Chem. Soc. Rev.* **2012**, *41*, 1261−1296. (c) Marvin-Sikkema, F. D.; Bont, J. A. M. Degradation of Nitroaromatic Compounds by Microorganisms. *Appl. Microbiol. Biotechnol.* **1994**, *42*, 499−507. (d) Mantha, R.; Taylor, K. E.; Biswas, N.; Bewtra, J. K. A Continuous System for Fe0 Reduction of Nitrobenzene in Synthetic Wastewater. *Environ. Sci. Technol.* **2001**, *35*, 3231−3236.

(2) (a) Schulte-Ladbeck, R.; Vogel, M.; Karst, U. Recent Methods for the Determination of Peroxide-Based Explosives. *Anal. Bioanal. Chem.* **2006**, *386*, 559−565. (b) Balakrishnan, V. K.; Halasz, A.; Hawari, J. Alkaline Hydrolysis of the Cyclic Nitramine Explosives RDX, HMX, and CL-20: New Insights into Degradation Pathways Obtained by the Observation of Novel Intermediates. *Environ. Sci. Technol.* **2003**, *37*, 1838−1843.

(3) (a) Thomas, S. W.; Joly, G. D.; Swager, T. M. Chemical Sensors Based on Amplifying Fluorescent Conjugated Polymers. *Chem. Rev.* **2007**, *107*, 1339−1386. (b) Germain, M. E.; Knapp, M. J. Optical Explosives Detection: from Color Changes to Fluorescence Turn-On. *Chem. Soc. Rev.* **2009**, *38*, 2543−2555. (c) Riskin, M.; Tel-Vered, R.; Bourenko, T.; Granot, E.; Willner, I. Imprinting of Molecular Recognition Sites through Electropolymerization of Functionalized Au Nanoparticles: Development of an Electrochemical TNT Sensor Based on π-Donor−Acceptor Interactions. *J. Am. Chem. Soc.* **2008**, *130*, 9726−9733.

(4) Woodfin, R. L. *Trace Chemical Sensing of Explosives*; John Wiley & Sons Inc.: Hoboken, NJ, 2007.

(5) (a) Luggar, R. D.; Farquharson, M. J.; Horrocks, J. A.; Lacey, R. J. Multivariate Analysis of Statistically Poor EDXRD Spectra for the Detection of Concealed Explosives. *X-Ray Spectrom.* **1998**, *27*, 87−94. (b) Hodyss, R.; Beauchamp, J. L. Multidimensional Detection of Nitroorganic Explosives by Gas Chromatography-Pyrolysis-Ultraviolet Detection. *Anal. Chem.* **2005**, *77*, 3607−3610. (c) Kim, T. H.; Lee, B. Y.; Jaworski, J.; Yokoyama, K.; Chung, W.-J.; Wang, E.; Hong, S.; Majumdar, A.; Lee, S.-W. Selective and Sensitive TNT Sensors Using Biomimetic Polydiacetylene-Coated CNT-FETs. *ACS Nano* **2011**, *5*, 2824−2830. (d) Schramm, E.; Hölzer, J.; Pütz, M.; Schulte-Ladbeck, R.; Schultze, R.; Sklorz, M.; Ulrich, A.; Wieser, J.; Zimmermann, R. Real-Time Trace Detection of Security-Relevant Compounds in Complex Sample Matrices by Thermal Desorption−Single Photon Ionization−Ion Trap Mass Spectrometry (TD-SPI-ITMS) Spectrometry (TD-SPI-ITMS). *Anal. Bioanal. Chem.* **2009**, *395*, 1795−1807. (e) Stępień, M.; Donnio, B.; Sessler, J. L. Supramolecular Liquid Crystals Based on Cyclo[8]pyrrole. *Angew. Chem., Int. Ed.* **2007**, *46*, 1431−1435. (f) Zhang, Y.; Tan, Y.-W.; Stormer, H. L.; Kim, P. Experimental Observation of the Quantum Hall Effect and Berry's Phase in Graphene. *Nature* **2005**, *438*, 201−204.

(6) (a) Nie, H.; Zhao, Y.; Zhang, M.; Ma, Y.; Baumgarten, M.; Mullen, K. Detection of TNT Explosives with a New Fluorescent Conjugated Polycarbazole Polymer. *Chem. Commun.* **2011**, *47*, 1234−1236. (b) Toal, S. J.; Trogler, W. C. Polymer Sensors for Nitroaromatic Explosives Detection. *J. Mater. Chem.* **2006**, *16*, 2871−2883.

(7) (a) Zhou, Q.; Swager, T. M. Method for Enhancing the Sensitivity of Fluorescent Chemosensors: Energy Migration in Conjugated Polymers. *J. Am. Chem. Soc.* **1995**, *117*, 7017−7018. (b) Zhao, D.; Swager, T. M. Sensory Responses in Solution vs Solid

State: A Fluorescence Quenching Study of Poly(iptycenebutadiynylene)s. *Macromolecules* **2005**, *38*, 9377−9384.
(8) (a) Sanchez, J. C.; DiPasquale, A. G.; Rheingold, A. L.; Trogler, W. C. Synthesis, Luminescence Properties, and Explosives Sensing with 1,1-Tetraphenylsilole- and 1,1-Silafluorene-vinylene Polymers. *Chem. Mater.* **2007**, *19*, 6459−6470. (b) Sohn, H.; Sailor, M. J.; Magde, D.; Trogler, W. C. Detection of Nitroaromatic Explosives Based on Photoluminescent Polymers Containing Metalloles. *J. Am. Chem. Soc.* **2003**, *125*, 3821−3830. (c) Martinez, H. P.; Grant, C. D.; Reynolds, J. G.; Trogler, W. C. Silica Anchored Fluorescent Organosilicon Polymers for Explosives Separation and Detection. *J. Mater. Chem.* **2012**, *22*, 2908−2914. (d) Germain, M. E.; Knapp, M. J. Discrimination of Nitroaromatics and Explosives Mimics by a Fluorescent Zn(salicylaldimine) Sensor Array. *J. Am. Chem. Soc.* **2008**, *130*, 5422−5423.
(9) Shu, W.; Guan, C.; Guo, W.; Wang, C.; Shen, Y. Conjugated Poly(aryleneethynylenesiloles) and Their Application in Detecting Explosives. *J. Mater. Chem.* **2012**, *22*, 3075−3081.
(10) Hu, X.-M.; Chen, Q.; Zhou, D.; Cao, J.; He, Y.-J.; Han, B.-H. One-Step Preparation of Fluorescent Inorganic-Organic Hybrid Material Used for Explosive Sensing. *Polym. Chem.* **2011**, *2*, 1124−1128.
(11) Kartha, K. K.; Babu, S. S.; Srinivasan, S.; Ajayaghosh, A. Attogram Sensing of Trinitrotoluene with a Self-Assembled Molecular Gelator. *J. Am. Chem. Soc.* **2012**, *134*, 4834−4841.
(12) (a) He, G.; Yan, N.; Yang, J.; Wang, H.; Ding, L.; Yin, S.; Fang, Y. Pyrene-Containing Conjugated Polymer-Based Fluorescent Films for Highly Sensitive and Selective Sensing of TNT in Aqueous Medium. *Macromolecules* **2011**, *44*, 4759−4766. (b) Du, H.; He, G.; Liu, T.; Ding, L.; Fang, Y. Preparation of Pyrene-Functionalized Fluorescent Film with a Benzene Ring in Spacer and Sensitive Detection to Picric Acid in Aqueous Phase. *J. Photochem. Photobiol., A* **2011**, *217*, 356−362.
(13) Lee, Y. H.; Liu, H.; Lee, J. Y.; Kim, S. H.; Kim, S. K.; Sessler, J. L.; Kim, Y.; Kim, J. S. Dipyrenylcalix[4]arene—A Fluorescence-Based Chemosensor for Trinitroaromatic Explosives. *Chem.—Eur. J.* **2010**, *16*, 5895−5901.
(14) Zyryanov, G. V.; Palacios, M. A.; Anzenbacher, P. Simple Molecule-Based Fluorescent Sensors for Vapor Detection of TNT. *Org. Lett.* **2008**, *10*, 3681−3684.
(15) Peng, Y.; Zhang, A.-J.; Dong, M.; Wang, Y.-W. A Colorimetric and Fluorescent Chemosensor for the Detection of an Explosive-2,4,6-trinitrophenol (TNP). *Chem. Commun.* **2011**, *47*, 4505−4507.
(16) Germain, M. E.; Vargo, T. R.; McClure, B. A.; Rack, J. J.; Van Patten, P. G.; Odoi, M.; Knapp, M. J. Quenching Mechanism of Zn(Salicylaldimine) by Nitroaromatics. *Inorg. Chem.* **2008**, *47*, 6203−6211.
(17) (a) Shanmugaraju, S.; Joshi, S. A.; Mukherjee, P. S. Fluorescence and Visual Sensing of Nitroaromatic Explosives Using Electron Rich Discrete Fluorophores. *J. Mater. Chem.* **2011**, *21*, 9130−9138. (b) Chakrabarty, R.; Mukherjee, P. S.; Stang, P. J. Supramolecular Coordination: Self-Assembly of Finite Two- and Three-Dimensional Ensembles. *Chem. Rev.* **2011**, *111*, 6810−6918.
(18) Venkatramaiah, N.; Kumar, S.; Patil, S. Fluoranthene Based Fluorescent Chemosensors for Detection of Explosive Nitroaromatics. *Chem. Commun.* **2012**, *48*, 5007−5009.
(19) Sheldrick, G. M. A Short History of SHELX. *Acta Crystallogr., Sect. A: Found. Crystallogr.* **2008**, *64*, 112−122.
(20) Farrugia, L. ORTEP-3 for Windows. *J. Appl. Crystallogr.* **1997**, *30*, 565.
(21) Farrugia, L. WinGX Suite for Small-Molecule Single-Crystal Crystallography. *J. Appl. Crystallogr.* **1999**, *32*, 837−838.
(22) Frisch, M. J.; Trucks, G. W.; Schlegel, H. B.; Scuseria, G. E.; Robb, M. A.; Cheeseman, J. R.; Montgomery, J. A.; Vreven, T.; Kudin, K. N.; Burant, J. C.; et al. *Gaussian 03*, revision C.02; Gaussian, Inc.: Wallingford, CT, 2004.
(23) Venkatramaiah, N.; Kumar, S.; Patil, S. Femtogram Detection of Explosive Nitroaromatics: Fluoranthene-Based Fluorescent Chemosensors. *Chem.—Eur. J.* **2012**, *18*, 14745−14751.
(24) Walker, W.; Veldman, B.; Chiechi, R.; Patil, S.; Bendikov, M.; Wudl, F. Visible and Near-Infrared Absorbing, Low Band Gap Conjugated Oligomers Based on Cyclopentadieneones. *Macromolecules* **2008**, *41*, 7278.
(25) Hull, J. W., Jr.; Romer, D. R.; Podhorez, D. E.; Ash, M. L.; Brady, C. H. Development of Potential Manufacturing Routes for Substituted Thiophenes − Preparation of Halogenated 2-Thiophenecarboxylic Acid Derivatives as Building Blocks for a New Family of 2,6-Dihaloaryl 1,2,4-Triazole Insecticides. *Beilstein J. Org. Chem.* **2007**, *3*, 23.
(26) Edwards, L. O.; Simpson, W. T. Polarizations of Electronic Transitions from Azimuthal Variation in Fluorescence Intensity with Application to Biphenyl. *J. Chem. Phys.* **1970**, *53*, 4237−4244.